THE EQUATION OF MOTION FOR SPERM FLAGELLA

ROBERT RIKMENSPOEL, *Department of Biological Sciences, State University of New York, Albany, New York 12222 U.S.A.*

ABSTRACT The equation of motion for sperm flagella, in which the elastic bending moment and the active contractile moment are balanced by the moment from the viscous resistance of the surrounding fluid, is solved for a wave solution that superimposes partial solutions. Substitution of the expression for the wave solution into the equation leads to an expression for the active contractile moment. This active moment can be decomposed into two parts. The first part describes an active moment that travels over the flagellum with the mechanical flagellar wave, the second part represents a moment in phase over the entire length of the flagellum, which decreases linearly towards the distal tip. The linear synchronous moment, to which an amount of traveling moment has been added as a perturbation, leads to wave solutions that closely resemble flagellar waves. Properties such as wavelength and wave amplitudes and also the shape of the waves in sea urchin sperm flagella at different frequencies are accurately described by the theory. The change in wave shape in sea urchin sperm flagella at raised viscosity is predicted well by the theory. The different wave properties caused in bull sperm flagella by different boundary conditions at the proximal junction are explained. When only a traveling active moment is present in a flagellum, the wave solutions describe waves of a small wavelength in a long flagellum. Some properties of the wave motion of long sperm flagella are derived from the theory and verified experimentally.

INTRODUCTION

In recent years much progress has been made toward an understanding of sperm flagellar motion. Detailed observations of motion patterns have been published (Brokaw, 1975; Gibbons, 1974; Wu et al., 1975; Rikmenspoel, 1965, 1978). The molecular mechanism that produces the forces necessary to maintain flagellar motion has been largely elucidated (Summers and Gibbons, 1971; Afzelius, 1974).

The extensive body of data has led investigators to develop often very intricate models in which properties of the flagellar motion are derived from a force-generating mechanism (Lubliner and Blum, 1971, 1972; Brokaw, 1972*a*, *b*; Brokaw and Rintala, 1974). However, the simple elegance of sperm flagellar movement, when viewed on slow-motion cinemicrographs, and the fact that its main characteristics appear to have remained unchanged through the course of evolution from invertebrates, such as sea urchins, to the higher mammals lead one to expect that very elementary physical principles are involved.

In this paper it will be shown that many properties of sperm flagellar motion can be derived from a simple equation of motion, without the need for a detailed model. The theory is applied to invertebrate, mammalian, and insect sperm. A preliminary publication of the results has been made (Skalafuris and Rikmenspoel, 1973).

THEORY

In a flagellum the internal active contractile moment, M_{act}, and the elastic bending moment, M_{el}, are balanced at each location by the moment due to the viscous resistance of the surrounding fluid, M_{visc}. The equation of motion is therefore

$$M_{el} + M_{act} = M_{visc}. \tag{1}$$

Eq. 1 is the simplest possible equation of motion. Other terms, such as moments due to shear stresses or internal viscous resistances might be added to it (Lubliner and Blum, 1971; Brokaw, 1972*a*), but none of the terms shown above can be omitted.

In the following the equilibrium position of the flagellum is assumed to be straight, and translational movements of the flagellum as a whole are neglected. This simplifies the algebra and the main results should not be affected.

The elastic moment M_{el} at a given location is $M_{el} = \rho IE$, where ρ is the local curvature, and IE is the stiffness of the flagellum. Adopting a coordinate system, as shown in Fig. 1, where x is the running coordinate and U is the deviation from the equilibrium position (the amplitude), we can write in small-amplitude approximation

$$M_{el} = IE\frac{\partial^2 U}{\partial x^2}. \tag{2}$$

All elements of the flagellum distal to x contribute to the viscous moment at x. In small-amplitude approximation, the drag force per unit length, F_D, due to the surrounding fluid at a point ξ (see Fig. 1) is $F_D = -k\partial U(\xi)/\partial t$, where k is the drag coefficient per unit length. With the lever $(\xi - x)$, the moment exerted by F_D at x is

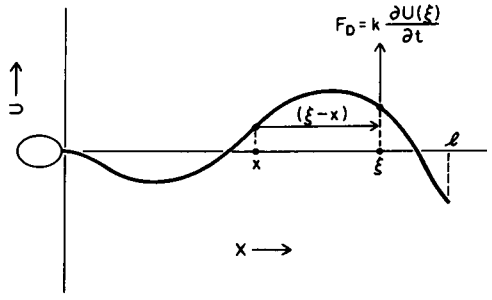

FIGURE 1 Coordinate system used in the calculations. F_D is the drag force per unit length due to the surrounding fluid.

$-k(\xi - x)\partial U(\xi)/\partial t$. The total viscous moment M_{visc} at x is therefore

$$M_{visc} = -\int_x^l k(\xi - x)\frac{\partial U(\xi)}{\partial t}d\xi. \tag{3}$$

Substitution of Eqs. 2 and 3 into Eq. 1 yields an equation of motion in which the active contractile moment M_{act} is as yet unspecified. The solutions of interest of this equation of motion are wave solutions. It has been shown experimentally (Rikmenspoel, 1965, 1978) that the transversal motion (in the U-direction) at each location x on a sperm flagellum is sinusoidal in time and can be represented by a single frequency, f. If we assume that the superposition principle holds for this case, a wave solution for the equation of motion is the sum of a series, each term of which represents a particular solution. The wave solution $U(x, t)$ can thus be written as

$$U(x,t) = \sum_n A_n e^{i(\omega t + \alpha_n x)} \quad (n = 1, 2—), \tag{4}$$

where $\omega = 2\pi f$ is the circle frequency of the flagellar wave, α_n is the wave number, and A_n the amplitude of the n^{th} term.

Substituting Eq. 4 into Eq. 2 gives for the elastic moment:

$$M_{el} = -IE\sum_n A_n\alpha_n^2 e^{i(\omega t + \alpha_n x)} \quad (n = 1, 2,—). \tag{5}$$

After substitution of Eq. 4 into Eq. 3 the integral in the right-hand part can be evaluated by repeated partial integration, resulting in

$$M_{visc} = -\sum_n \frac{k\omega A_n}{\alpha_n}\left[(l - x)e^{i\alpha_n l} + \frac{i}{\alpha_n}e^{i\alpha_n l} - \frac{i}{\alpha_n}e^{i\alpha_n x}\right]e^{i\omega t} \quad (n = 1, 2,—). \tag{6}$$

By inserting the expressions for M_{el} and M_{visc} of Eq. 5 and 6 respectively, into Eq. 1, and after rearranging the terms, an expression for M_{act} is found:

$$M_{act} = e^{i\omega t}\left\{\sum_n A_n\alpha_n^2 e^{i\alpha_n x}\left[IE + \frac{ik\omega}{\alpha_n^4}\right] - \sum_n k\omega A_n \frac{e^{i\alpha_n l}}{\alpha_n}\left[(l - x) + \frac{i}{\alpha_n}\right]\right\}$$

$$(n = 1, 2,—). \tag{7}$$

An active contractile moment, M_{act}, of the form given in Eq. 7 will give a wave solution to the equation of motion, as shown in Eq. 4.

It can be seen in Eq. 7 that the active moment has two distinct parts. The first part, M_1:

$$M_1 = e^{i\omega t}\sum_n A_n\alpha_n^2 e^{i\alpha_n x}\left[IE + \frac{ik\omega}{\alpha_n^4}\right] \quad (n = 1, 2,—), \tag{8}$$

is a series in which each term depends on x as $\exp(i\alpha_n x)$. M_1 as defined in Eq. 8 is an active moment that travels along the flagellum with the flagellar wave given in Eq. 4. We shall refer to M_1 as a "traveling moment."

The second part of M_{act} is a series, M_2, in which each term has a linear dependency on x:

$$M_2 = -e^{i\omega t} \sum_n k\omega A_n \frac{e^{i\alpha_n l}}{\alpha_n} \left[(l - x) + \frac{i}{\alpha_n}\right] \quad (n = 1, 2, —). \tag{9}$$

This represents an active moment, synchronous in phase at all locations on the flagellum, which will be referred to as a "standing moment." We shall investigate the effects of the standing and the traveling moment below.

The Standing Moment

If only the standing moment M_2 of Eq. 9 is present in a flagellum, the traveling moment M_1 of Eq. 8 must vanish. Since then $M_1 = 0$ for every x between 0 and l, every term of the series of Eq. 8 must vanish. For all finite values of α_n, therefore, $A_n = 0$ (which represent trivial solutions), except for those α_n for which

$$IE + ik\omega/\alpha_n^4 = 0. \tag{10}$$

This leads to four nontrivial solutions with wave numbers α_n:

$$\alpha_n = (-ik\omega/IE)^{1/4} \quad (n = 1, —, 4). \tag{11}$$

The four solutions represented by Eq. 11 are identical to the solutions found by Machin (1958) for a passive flagellum.

The active moment, M_{act}, now is

$$M_{act} = -e^{i\omega t} \sum_n k\omega A_n \frac{e^{i\alpha_n l}}{\alpha_n} \left(l - x + \frac{i}{\alpha_n}\right) \quad (n = 1, —, 4). \tag{12}$$

It may appear somewhat surprising that a standing moment, in synchronous phase at all locations, gives rise to a traveling wave of displacement in the flagellum. However, I have previously evaluated the active contractile moments in sea urchin and in bull sperm flagella (Rikmenspoel, 1971), and concluded that the active moments are in phase and linearly decreasing with x. Close inspection of Figs. 4C and 5C of Rikmenspoel (1971) also reveals that these standing active moments in both sea urchin and in bull sperm vanish at a point before the distal end of the tail. In sea urchin sperm with $l = 42\ \mu m$ the active moment vanishes at $x = 35\ \mu m$; in bull sperm, with $l = 60\ \mu m$, it does so at $x \approx 50\ \mu m$. This corresponds to the existence of an inert terminal piece on the sperm flagella, which has indeed been shown to exist in both species (Brokaw, 1974; Fawcett, 1961, 1966; Gray, 1955).

The active moments reported by Rikmenspoel (1971) can be approximated as

$$M_{act} = e^{i\omega t} m_0 (l - x - \delta), \tag{13}$$

where m_0 is the maximum value of the active moment at $x = 0$, and δ is the length of the inert terminal piece. Eq. 13 is strictly valid only for the active part of the flagellum, $0 < x < (l - \delta)$, since in the terminal piece $M_{act} = 0$. It should also be noted that Eq. 13 has been verified only for sea urchin and bull sperm flagella, and that its validity for e.g. cellular flagella is presently unknown. A comparison of Eqs. 12 and 13 gives two equations for the four amplitudes $A_n (n = 1, —, 4)$ with which the four wave solutions have to be combined:

$$\sum_n \frac{e^{i\alpha_n l}}{\alpha_n} A_n = \frac{-m_0}{k\omega} \quad (n = 1, —, 4), \tag{14}$$

and

$$\sum_n \frac{e^{i\alpha_n l}}{\alpha_n^2} A_n = \frac{-im_0\delta}{k\omega} \quad (n = 1, —, 4). \tag{15}$$

The two additional equations needed to determine the solution completely are obtained from the boundary conditions at the proximal end of the flagellum. If the sperm is unrestrained ("free") and the influence of the head is neglected, the viscous moment and its derivative with respect to x (the shearing force) have to vanish at $x = 0$. At $x = 0$ one finds from Eq. 5: $M_{el}(0) = -\exp(i\omega t) IE\Sigma A_n \alpha_n^2$ and from Eq. 13 $M_{act}(0) = \exp(i\omega t) m_0 (l - \delta)$. With $M_{visc}(0) = 0$, and from Eq. 1 one thus finds

$$\sum_n \alpha_n^2 A_n = \frac{m_0(l - \delta)}{IE} \quad (n = 1, —, 4). \tag{16}$$

The vanishing shearing force at $x = 0$ leads in an analogous way to

$$\sum_n \alpha_n^3 A_n = -\frac{im_0}{IE} \qquad (n = 1, —, 4). \tag{17}$$

In those cases where the head is fixed to the slide but is able to pivot ("hinged"), $M_{visc}(0) = 0$, and Eq. 16 holds, but Eq. 17 must be replaced by the condition that $U(0, t) = 0$ or

$$\sum_n A_n = 0 \quad (n = 1, —, 4). \tag{18}$$

If the head is firmly fixed ("clamped"), both the amplitude and its derivative with respect to x vanish at $x = 0$, and the boundary conditions are Eq. 18 with

$$\sum_n \alpha_n A_n = 0 \quad (n = 1, —, 4). \tag{19}$$

The wave in the flagellum due to the active moment of Eq. 13 is now completely determined by Eqs. 11, 14, and 15 with in addition Eqs. 16 and 17 for free-

swimming sperm, Eqs. 16 and 18 for hinged sperm, or Eqs. 18 and 19 for clamped sperm. In all cases the solutions are proportional to the magnitude m_0 of the active moment.

It has usually been thought that in sperm flagella an active contractile moment is present that is maximal near the crest of the flagellar wave, and travels along the flagellum with the wave of displacement. From an analogy with cilia (Rikmenspoel and Rudd, 1973) it has recently been argued that this traveling active moment should have a magnitude much smaller than that of the standing moment considered above. This makes it logical to investigate the influence of such a traveling active moment by introducing it as a perturbation to the treatment above.

A traveling active moment that moves with the wave of displacement is represented by M_1, as defined in Eq. 8. The perturbation is most easily introduced not by setting $IE + ik\omega/\alpha_n^4 = 0$ (compare Eq. 10), but by letting it have a "small" value, $\beta e^{i\Psi}$. If we write $p = \beta/IE$, the wave numbers α_n for the four solutions given in Eq. 11 now become

$$\alpha_n = \left[\frac{-ik\omega}{IE(1 + pe^{i\Psi})}\right]^{1/4} \quad (n = 1, —, 4). \tag{20}$$

Of the four equations for solving the four A_n, Eqs. 14 and 15 remain unchanged by the perturbation. In the boundary conditions, Eq. 16 is to be replaced by

$$\sum_n \alpha_n^2 A_n = \frac{m_0(l - \delta)}{IE(1 + pe^{i\Psi})} \quad (n = 1, —, 4), \tag{21}$$

and Eq. 17 by

$$\sum_n \alpha_n^3 A_n = -\frac{im_0}{IE(1 + pe^{i\Psi})} \quad (n = 1, —, 4). \tag{22}$$

In the treatment described above the perturbation by the traveling active moment, M_1, can be investigated in a simple way via the dimensionless constant p. The moment M_1 is now given by

$$M_1 = e^{i\omega t} IEpe^{i\Psi} \sum_n \alpha_n^2 A_n e^{i\alpha_n x} \quad (n = 1, —, 4). \tag{23}$$

Eq. 23 shows that the magnitude of the traveling moment M_1 is proportional to p. The computed wave amplitudes represented by $A_n (n = 1, —, 4)$ are all proportional to the magnitude of the standing moment m_0. A comparison of Eqs. 4 and 23 indicates that the constant p can be interpreted as representing a proportionality constant of the magnitudes of the traveling and the standing moment. The quantitative results related below in the sections Invertebrate Sperm and Bull Sperm reveal that when $p = 1$, the ratio of the magnitudes of M_1 and M_2 is not far from 1.

If $B(x) = \sum_n A_n \exp(i\alpha_n x)$, the real wave solution $U_r(x, t)$ to be compared with

experimental data can be written as

$$U_r(x,t) = A(x)\cos[\omega t + \alpha(x)], \tag{24}$$

where $A(x) = 2 \mid B(x) \mid$, and $\alpha(x) = \arctan[-ImB(x)/ReB(x)]$.

Of the quantities occurring in the theory above, independent measurements or estimates of k, ω, l, δ, IE, and m_0 are available for invertebrate sperm (sea urchin and *Ciona*) and for mammalian sperm (bull). Wave solutions can therefore be directly computed as a function of the term $p\exp(i\Psi)$ for comparison with observed motions for these sperm. It should be noted that the term $p\exp(i\Psi)$ occurs in a different way in the equations derived for the three different boundary conditions, free, hinged, and clamped. It is therefore to be expected that the influence of the term $p\exp(i\Psi)$ will manifest itself in a different way for these boundary conditions.

Computations for arriving at the wave solutions, Eq. 24, were programmed for a Univac 1110 computer (Sperry Univac, Blue Bell, Pa.). The program made use of a complex matrix inversion routine provided by the Courant Institute for Applied Mathematics, New York.

The Travelling Moment

If only the traveling moment M_1 of Eq. 8 is present in a flagellum, the standing moment M_2 of Eq. 9 must vanish. For M_2 to vanish at all values of x, every term of the series in Eq. 9 has to vanish. This can occur if all amplitudes A_n vanish, leading to trivial solutions. A nontrivial solution can be derived, however, as follows.

If A is the amplitude and α the wave number of a nontrivial solution (omitting the index n for simplicity of notation), the expression for M_2 (compare Eq. 9) can be rewritten as:

$$M_2 = -k\omega A\, e^{i(\omega t + \alpha l)}\left[\frac{(l - x)}{\alpha} + \frac{i}{\alpha^2}\right]. \tag{25}$$

M_2 in Eq. 25 will vanish when both $(l - x)/\alpha$ and $1/\alpha^2$ are "sufficiently small." It is not a priori possible, though, to define how small $(l - x)/\alpha$ and $1/\alpha^2$ should be for M_2 to be considered vanished.

In the Appendix it is shown that M_2 in Eq. 25 can only vanish when $1/\alpha \ll l$. The Appendix also explains how the necessary condition $1/\alpha \ll l$ is related to the condition mentioned above that $(l - x)/\alpha$ and $1/\alpha^2$ be sufficiently small.

Spermatozoa which have wave motion but in which no linear standing motion is present (requiring $1/\alpha \ll l$) should thus display waves with a wavelength $\lambda = 2\pi/\alpha \ll l$. Examples of spermatozoa that show waves of a wavelength much smaller than the flagellar length are known in certain species of insects (Phillips, 1970, 1974; Chapman, 1969). The sperm of *Drosophila,* for example, or cricket, are 800–1,200-μm long and display waves of 10–30 μm length. It appears worthwhile therefore to investigate whether these long insect sperm do indeed represent the case discussed above of a finite wave solution in the absence of a standing active moment.

A direct measurement of the active moments in the long insect sperm, which would show whether a standing moment were present or not, does not appear to be practical. As an alternative to this measurement, we will investigate the consequences to the characteristics of the wave motion of the mechanism in which M_2 vanishes due to $(l - x)/\alpha$ and $1/\alpha^2$ being sufficiently small.

The viscous moment M_{visc} for a sperm flagellum, given in Eq. 6 above, can be rewritten for the particular wave solution under consideration (omitting the index again) as:

$$M_{visc} = -k\omega A\, e^{i(\omega t + \alpha l)}\left[\frac{(l - x)}{\alpha} + \frac{i}{\alpha^2}\{1 - e^{i\alpha(x-l)}\}\right]. \tag{26}$$

In the above expression the term $e^{i\alpha(x-l)}$ has the magnitude of 1, and $\{1 - e^{i\alpha(x-l)}\}$ has therefore also the magnitude of 1. A nonvanishing wave solution with a wave number α such that $(l - x)/\alpha$ and $1/\alpha^2$ are sufficiently small to cause M_2 in Eq. 25 above to vanish, will therefore also cause M_{visc} in Eq. 26 to vanish. In that case the equation of motion (Eq. 1) is reduced to $M_{el} + M_1 = 0$, or

$$IE\frac{\partial^2 U}{\partial x^2} + M_1 = 0. \tag{27}$$

Eq. 27 is not a partial differential equation, but an ordinary one. Consequently Eq. 27 describes a local behavior of the flagellum and no longer the flagellum as a whole. Eq. 27 can be integrated directly, yielding $U = -(1/IE)\iint M_{act}$ and showing that the flagellar wave follows the local active contractile moment. In flagella for which Eq. 27 is valid, one can expect therefore that different parts show different waves reflecting variations in M_{act} at various locations. It should be noted that this does not imply that a sliding filament mechanism is not operating in such sperm flagella, but only that the active mechanism is not coordinated over the entire length.

The simplified equation of motion (Eq. 27) does not contain the effects of the viscous drag of the fluid surrounding the sperm. It can therefore be expected that the wave motion of sperm, for which $M_2 = 0$ and for which Eq. 27 holds, should not vary when the viscosity of the surrounding fluid is raised.

Summarizing the above, we can say that the consequences of a vanishing standing moment in a motile sperm are: (*a*) the wavelength should be small compared to the flagellar length; (*b*) different sections of a flagellum can show different waves; and (*c*) the wave properties should not depend on the external viscosity. In the section on cricket sperm below it will be shown that these characteristics are indeed observed experimentally in long insect spermatozoa.

EXPERIMENTAL DATA AND METHODS

Invertebrate Sperm

Movement characteristics of sea urchin sperm at normal viscosity (1.4 cP) were taken from a detailed description published recently (Rikmenspoel, 1978). Tracings of flagellar wave forms

were obtained from the same cinemicrographs as the above-mentioned description. The data on the motion of sea urchin and *Ciona* sperm at raised viscosity were from Brokaw (1966).

Bull Sperm

Motion data of free-swimming bull spermatozoa at 37°C were obtained from Rikmenspoel (1965). Only data pertaining to sperm with a flat (two-dimensional) flagellar wave were used. Characteristics of the motion of bull sperm with different boundary conditions (clamped or hinged at the head) and with reduced flagellar frequency wave have not appeared in the literature. These data were obtained from films made in this laboratory especially for that purpose.

Bull spermatozoa were generously provided by the Eastern Artificial Insemination Cooperative at Ithaca, N.Y. After ejaculation, the semen was diluted and cooled to 4°C as previously described (Rikmenspoel et al., 1973). For experiments, sperm were washed twice and suspended to a final concentration of approximately 10^6/ml, as previously described (Lindemann and Rikmenspoel, 1971). Some sperm stick to the slide after this washing procedure, some with the head firmly attached (clamped), some able to pivot around the attachment point (hinged). In a number of preparations the sperm were demembranated by extraction for 15 s in 0.02% solution of Triton X-100 (Rohm & Haas Co., Philadelphia, Penn.), as previously described (Lindemann and Gibbons, 1975). These extracted sperm were reactivated with 3 mM externally added ATP.

A range of frequencies of the bull sperm flagellar motion was obtained by observing the sperm intact at 37°C, demembranated at 37°C, and intact at a room temperature of 21°C. The range thus covered was approximately from 2 to 24 cycle/s, for all three types of boundary conditions (free, clamped, and hinged).

Cinemicrographs of the preparations in the various conditions were made at 200 frames/s (fps) as previously described (Rikmenspoel et al., 1973). Analysis was done on spermatozoa whose flagellar waves were flat. This eliminates errors due to the rotation of sperm and due to projection effects. The method of analysis has been described previously in detail (Rikmenspoel, 1965).

Cricket Sperm

Spermatozoa were obtained by dissecting and puncturing the testes of male crickets. The spermatozoa were suspended in insect Ringer solution (IRS) (Fielden, 1960). The viscosity of the suspension medium was raised when desired by the addition of Ficoll (Sigma Chemical Co., St. Louis, Mo.). The cricket sperm were mixed very gently into the IRS, especially when high-viscosity IRS was used, to avoid rupture of the very long (up to 800 μm) sperm. Cinemicrographs of the preparations were made at 50 fps at a room temperature of 21°C.

The viscosity of the suspensions was measured with a falling ball viscometer previously described (Lindemann and Rikmenspoel, 1972).

RESULTS

Invertebrate Sperm

Sea urchin sperm flagella are thin cylinders of 41–43 μm long (Brokaw, 1966; Rikmenspoel, 1978). A thin, inert terminal piece of 5–8 μm long occurs distally to the flagellum (Gray, 1955). The force-producing structures (the dynein-tubulin fibers) terminate several micrometers before the end of the flagellum (Satir, 1968). For the present calculations we have taken a length $l = 45$ μm and an inert length $\delta = 10$ μm. The drag coefficient per unit length, calculated with the formalism of Gray and Hancock (1955) is $k = 1.6 \times 10^{-2}$ dyn cm^{-2} s (Rikmenspoel, 1966).

TABLE I

WAVELENGTH AT VARIOUS FREQUENCIES OF SEA URCHIN SPERM COMPUTED AS A FUNCTION OF THE MAGNITUDE OF THE TRAVELING ACTIVE MOMENT, REPRESENTED BY p.

ω	Frequency	Wavelength			Exp. value
		$p = 0$	$p = 0.6$	$p = 1.5$	
rad/s	*cycle/s*		*μm*		
60	9.5	30	33	35.5	34
120	19	26	28	29	27
180	28.6	24.5	25	26	24.5
240	38.2	23	24	24	24
300	47.7	22.5	23	23	23

The experimental values were obtained by interpolation of the data in Fig. 4.

There appears to be general agreement now that the stiffness IE of an axoneme, of which the sea urchin sperm flagellum is an example, is approximately 10^{-13} dyn cm^2 (Rikmenspoel, 1971, 1976; Brokaw, 1972*b*; Lindemann, 1975). All calculations below were done with a value $IE = 10^{-13}$ dyn cm^2.

In the literature detailed descriptions of the motions are available only for free-swimming sperm. Accordingly, all calculations were carried out for the free boundary conditions.

With the above values for l, δ, k, and IE, wave solutions were computed, driven only by the linear standing moment M_2 ($p = 0$). Traveling waves were obtained at all frequencies between 9 and 50 cycle/s. The wavelength of these waves was close to the experimental value of the wavelength, as shown in Table I. When the value of m_0 (the magnitude of the linear standing moment) was adjusted so that the computed amplitude at $x = 15$–20 μm agreed with the experimental one, the amplitude of the computed wave in the distal part of the flagellum was too small at all flagellar frequencies. This is illustrated in Fig. 2 for a sperm at a flagellar frequency of 8.2 cycle/s and for one at 43 cycle/s.

The computed amplitudes near the proximal junction ($x = 0$) increased steeply, because a sharp curvature occurred in the computed wave shapes near $x = 0$. In the small amplitude approximation used in the present calculations, this sharp curvature leads to a large value of the amplitude. In the observed wave patterns of sea urchin sperm the large increase in curvature near the proximal junction is indeed present (Rikmenspoel, 1978). The constant length of a real flagellum limits the amplitude, however. The sharp increase in curvature near $x = 0$ in the computed waves has therefore been taken as reflecting the observed increase in curvature there.

When the perturbation by a traveling active moment M_1 is introduced ($p > 0$) the wavelength of the computed waves changes little, as shown in Table I. At each value of p there was only one value of the phase Ψ for which smooth, traveling wave patterns were obtained. This value of Ψ, found in each case by trial and error, varied from 4.8 to 5.3 rad for the different cases shown in Table I. It should be noted that Ψ repre-

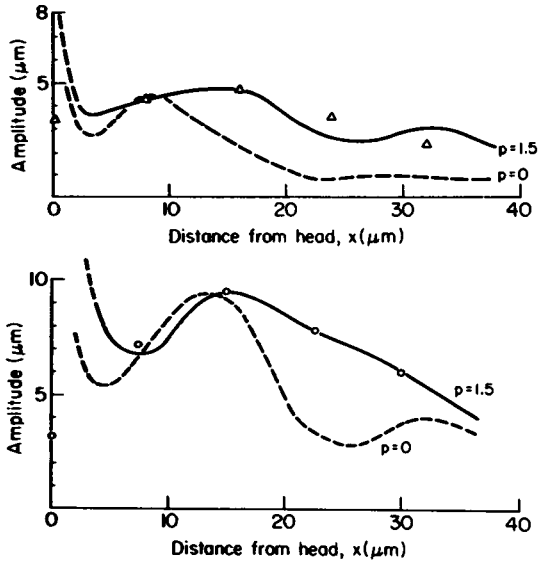

FIGURE 2 Amplitudes of computed waves for a standing active moment only ($p = 0$) and for a standing plus a traveling active moment ($p = 1.5$), for two sea urchin spermatozoa with a flagellar frequency of 8.2 (bottom) and 43 cycle/s (top). Δ and 0 are measured values.

sents the phase angle between curvature of the flagellum and the traveling active moment M_1, as can be seen by comparing Eqs. 2, 5, and 23 above. It can be expected that a smooth wave solution will only be obtained at the proper phase relation between the curvature and M_1.

When $p > 0$, the computed amplitude in the distal part of the wave was increased

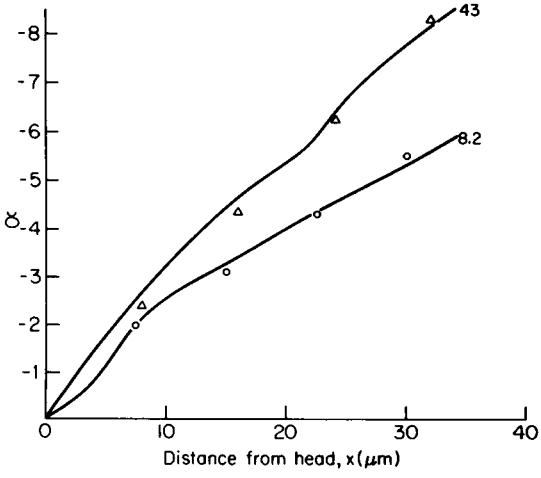

FIGURE 3 Computed $\alpha(x)$ for two sea urchin spermatozoa with a flagellar frequency of 8.2 (0) and 43 cycle/s (Δ). Δ and 0 are measured values.

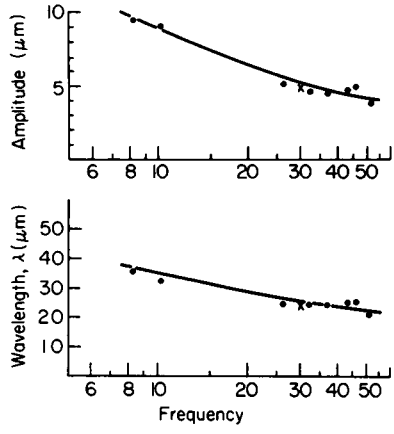

FIGURE 4 Amplitude and wavelength of sea urchin spermatozoa as a function of the flagellar frequency (cycle/s). The line in the top graph (amplitude) was drawn by eye through the data points. The line in the lower graph (wavelength) was computed with $p = 1.5$.

compared to that with $p = 0$. Smooth wave solutions could be computed with values of p of up to approximately 2. For $p > 2$ the computed wave solutions became irregular. Fig. 2 shows that for $p = 1.5$ the amplitudes of the computed waves at 8.2 and 43 cycle/s were close to the observed ones. The progression of the waves with $p = 1.5$, as described by the function $\alpha(x)$ of Eq. 24 above, is shown for the two sperm at 8.2 and 43 cycle/s, respectively, in Fig. 3. It can be seen in Fig. 3 that although the computed lines deviate little from the data points, the shape of the computed $\alpha(x)$'s is less smooth than the data points suggest. This is undoubtedly due to the fact that the computed curves are a combination of four discrete solutions, which represent a simplification of the real flagellum.

The value of x for which $\alpha(x) = 2\pi$ represents the wavelength of the computed wave. Fig. 4 (bottom) shows the computed wavelength, as a function of the frequency, for a constant value of $p = 1.5$ over the entire range. The agreement with the data points shown in Fig. 4 is quite good.

TABLE II

STANDING MOMENT M_2, TRAVELING MOMENT M_1 AND TOTAL ACTIVE MOMENT M_{act} COMPUTED FOR SEA URCHIN SPERM AT VARIOUS FREQUENCIES

ω	Frequency	Moments at $x = 0$		
		M_2	M_1	M_{act}
rad/s	*cycle/s*		10^{-10} *dyn cm*	
60	9.5	7.2	4.7	11.6
120	19	4.9	3.4	8
180	28.6	4.9	3.4	8.5
240	38.2	5.1	4.1	8.8
300	47.7	5.5	4.4	9.5

Fig. 4 (top) shows the maximum amplitude of the sea urchin sperm flagellar wave. The line in Fig. 4 (top) was drawn by eye through the measured points. It was explained under Theory that the amplitude of the computed solutions is proportional to the magnitude m_0 of the standing moment M_2. In the calculations m_0 was therefore adjusted in each case so that the computed amplitude conformed to the line drawn in Fig. 4 (top). With the fixed value of $p = 1.5$, the active moments M_1, M_2, and $M_{act} = M_1 + M_2$ were then evaluated from Eqs. 13 and 23 above. Table II shows the magnitude of M_1, M_2, and the total active moment M_{act} at the head flagellar junction, evaluated for the different flagellar frequencies. It can be seen in Table II that no clear relation between M_{act} and the flagellar frequency exists. It is somewhat surprising to notice in Table II that the traveling moment M_1 is not small compared to the standing moment M_2. It appears, however, that the perturbation method of introducing M_1 remains applicable at sizable magnitudes of M_1. Fig. 5 (left) shows the magnitude of M_1 and M_2 as a function of the location on the flagellum, computed for a sperm at $f = 38.2$ cycle/s. It can be seen that due to the changing phase relation between M_1 and M_2 along the flagellum the magnitude of the total active moment M_{act} is not equal to the sum of the magnitudes of M_1 and M_2. Fig. 5 (right) shows the phase relations between the wave of displacement $U(x, t)$, and the moments M_1, M_2, and M_{act}. The phase of M_{act} is almost constant as a function of x. Both the magnitude and the phase of M_{act} as shown in Fig. 5 are similar to those shown earlier (Fig. 4 of Rikmenspoel, 1971) and obtained by a direct evaluation of M_{visc} and M_{el} from motion patterns.

Fig. 6 shows tracings of observed motion of two sperm at 8.2 and 43 cycle/s, and wave forms computed for those frequencies. Even though the representation in the computed wave forms deviates in details from the observed ones, the general aspect of the computed waves is close to the observed ones.

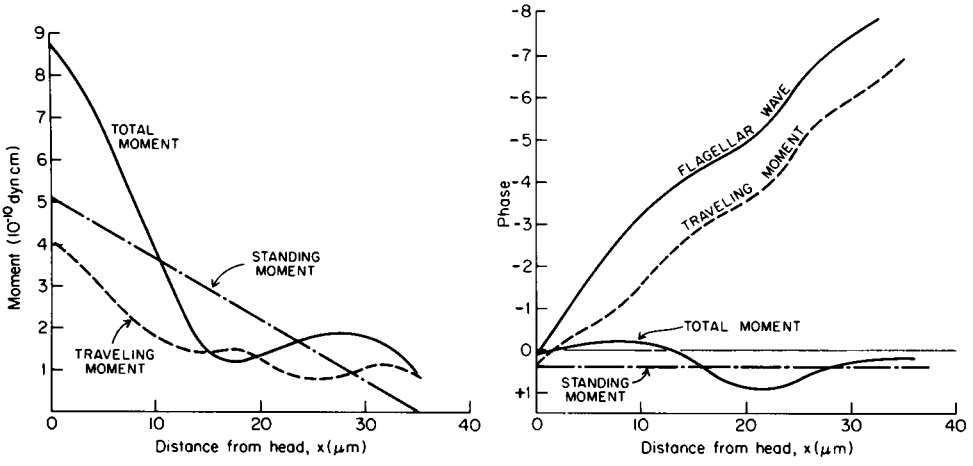

FIGURE 5 Left: Magnitude of the standing moment M_2, the traveling moment M_1, and the total active moment M_{act} for a typical sea urchin sperm with $f = 38$ cycle/s. Right: Phase of the flagellar wave $U(x, t)$, and the moments M_1, M_2, and M_{act} for the sea urchin sperm represented at the left. The phases are normalized to the phase of $U(0, t)$, taken as zero.

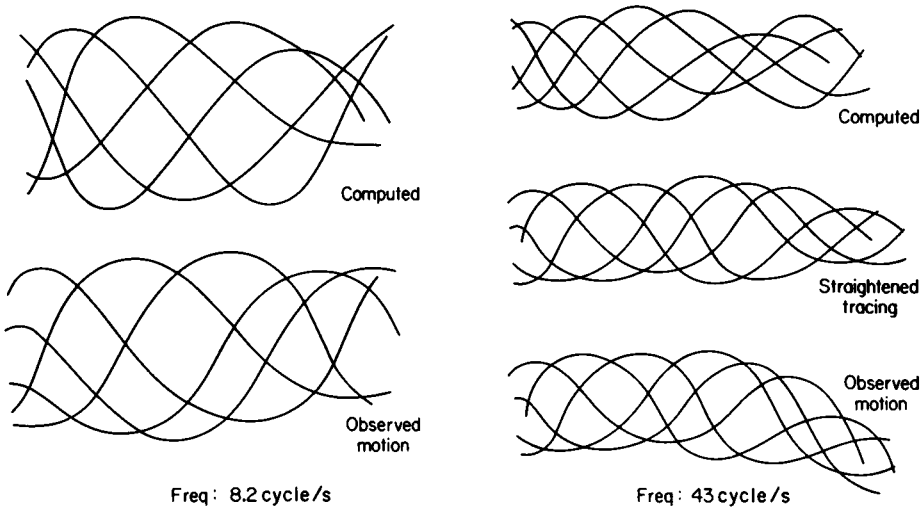

FIGURE 6 Computed and observed wave forms of the flagellum of two sea urchin sperm with a flagellar frequency of 8.2 (left) and 43 cycle/s (right). The observed tracing at the right was "straightened" by cutting the tracings in vertical strips and remounting it as shown. The proximal junction of the flagella in this figure, and in Figs. 8, 13, and 16 is to the left. The proximal 3–5 μm of the computed wave forms in this figure and in Fig. 8 are omitted.

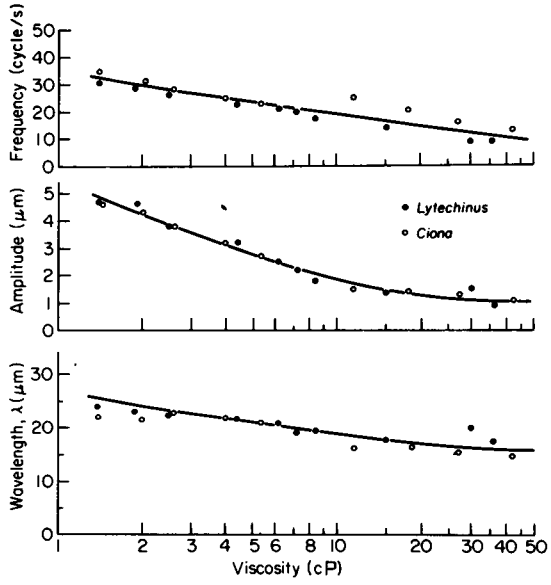

FIGURE 7 Average flagellar frequency, average amplitude, and average wavelength of sea urchin and *Ciona* sperm as a function of the external viscosity. The lines in the top and middle graph were drawn by eye through the data points; the line for the wavelength was computed with $p = 1.5$.

TABLE III

AVERAGE FLAGELLAR FREQUENCY, f, STANDING MOMENT M_2, TRAVELING MOMENT M_1 AND TOTAL ACTIVE MOMENT M_{act} FOR INVERTEBRATE SPERM AS A FUNCTION OF VISCOSITY

Viscosity	f	Moments at $x = 0$		
		M_2	M_1	M_{act}
cP	*cycle/s*		10^{-10} *dyn cm*	
1.4	32	5.8	3.8	9.4
2.8	27.5	5.2	4.2	9
5.6	23	5.1	3.7	8.6
11.2	18.5	5.0	3.8	8.5
22.4	14	5.0	3.4	8.1
44.8	9.5	5.0	3.4	8.1

Data on wave parameters and wave shapes of sea urchin and *Ciona* sperm as a function of the viscosity of the external medium, η, have been published by Brokaw (1966). Fig. 7 shows the average frequency of the flagellar beat (top), the average wave amplitude (middle), and the average flagellar wavelength (bottom) as a function of η. For computations the average frequency was adopted as shown in Fig. 7 (top) by the line drawn through the experimental points. For all values of η, the magnitude of m_0 was adjusted so that the computed amplitude was equal to that shown by the drawn line in Fig. 7 (middle). The wavelength of the flagellar beat was then computed as a function of η, with a constant value of $p = 1.5$. All other quantities (l, δ, IE) were kept at the original value, but the drag coefficient k was corrected appropriately for the various viscosities.

Fig. 7 (bottom) shows the computed wavelength, λ, with the observed values. At $\eta = 1.4$ and 2.0 cP the computed wavelength is slightly higher than the observed one, but the overall trend of the data is well reproduced in the computed curve. Table III shows the magnitudes of M_1, M_2, and the total active moment M_{act} as a function of viscosity. All three moments are apparently approximately constant over the range of η.

Fig. 8 shows computed wave forms at raised viscosities of 6.2 and 44.8 cP, and tracings of the observed shapes. It can be seen that the variation of the amplitude of the waves along the flagellum and indeed the general wave shapes of the computed waves are close to the observed ones.

Bull Spermatozoa

Bull spermatozoa are bigger, more powerful, and mechanically stronger than sea urchin spermatozoa. It is thus possible to manipulate bull sperm, and to change effectively the boundary conditions at the proximal end. This appears not to have been attained reliably with the (invertebrate) sea urchin sperm.

The length of a bull sperm flagellum is 60 μm, with a terminal piece of approximately 5 μm. The proximal 10–12 μm of the flagellum, the midpiece, has an increased diam-

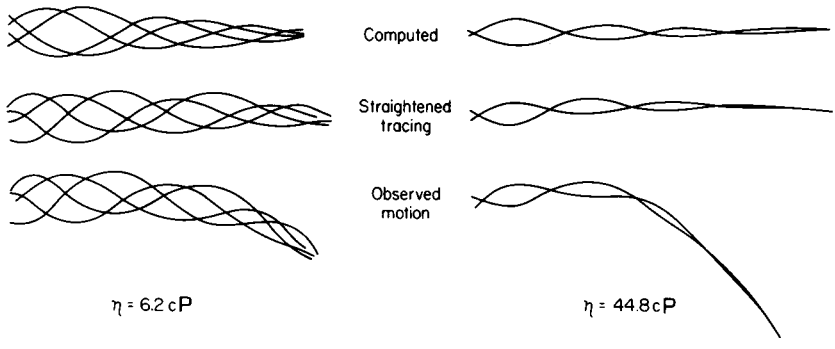

FIGURE 8 Observed and computed wave forms of sea urchin spermatozoa at a viscosity η of 6.2 (left) and 44.8 (right) cP. The procedure for straightening the observed tracings was explained at Fig. 6 above.

eter and apparently an increased stiffness (Phillips, 1972). The flagellum is tapered from the midpiece to the distal end (Fawcett, 1961, 1966). The coarse longitudinal fibers inside the flagellum, probably force-producing structures, are tapered towards the distal end, and terminate well before the distal tip (Fawcett, 1966; Nelson, 1962).

Calculations as outlined in the Theory section above, which apply to a cylindrical flagellum, necessarily have to be approximate for the bull sperm flagella. The stiffness of a bull sperm flagellum at the midpiece-flagellum junction has been reported as 1.8×10^{-12} dyn cm^2 (Rikmenspoel, 1965; Lindemann et al., 1973). In all calculations reported, a uniform stiffness of the flagellum of $IE = 1.8 \times 10^{-12}$ has been used; proximally to the midpiece-flagellum junction the stiffness was thus underestimated, distally it was overestimated. The length of the flagellum including the midpiece was taken as $l = 60$ μm. In the course of preliminary calculations, it appeared at a length of the inert terminal piece $\delta = 15$ μm, the smoothest wave solutions were obtained. For all calculations the value $\delta = 15$ μm was therefore maintained. The length of the inert piece is probably overestimated in the above value, but the tapering of the flagellum may to some extent be simulated by it. The drag coefficient, at the midpiece-flagellum junction has been reported as $k = 2.1 \times 10^{-2}$ dyn cm^{-2} s (Rikmenspoel, 1965), and this value was used throughout. At the distal part of the flagellum the effective viscous drag is reduced due to the taper and due to projection effects (Rikmenspoel, 1965), but no attempt to correct for this has been made.

In bull sperm flagella only one full wave or less is present (compared to one and a half waves in sea urchin sperm). Therefore the wavelength, defined as the value of x for which $\alpha(x) = 2\pi$, is not a suitable parameter. Instead the length of the first half wave, $\frac{1}{2}\lambda$, defined as that x for which $\alpha(x) = \pi$, has been used. For flagella at low frequency the rather straight section of the curves for $\alpha(x)$ in the proximal part of the flagellum was extrapolated to obtain a value for $\frac{1}{2}\lambda$ (compare Fig. 11 below).

CLAMPED BOUNDARY CONDITIONS The initial calculations showed that computed values of $\frac{1}{2}\lambda$ for clamped bull sperm flagella depended strongly on the amount of traveling active moment M_1. Furthermore, for all traveling moments M_1 correspond-

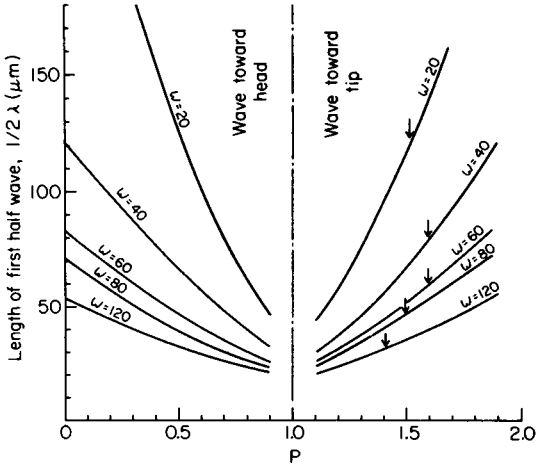

FIGURE 9 Computed length of the first half wave ($\frac{1}{2}\lambda$) for clamped bull sperm at various frequencies as a function of p. The arrows indicate the value of p corresponding to the value of $\frac{1}{2}\lambda$ shown by the line drawn in Fig. 10 below.

ing to a value of p between 0 and 1, the wave progression was towards the head, instead of towards the distal tip as is normally observed in sperm flagella. Fig. 9 shows the computed values of $\frac{1}{2}\lambda$ at various frequencies as a function of p. For all cases the optimal value of the phase angle Ψ was close to π. Solutions for values of p close to 1 could therefore not be computed. When $p > 1$ the direction in which the computed waves traveled was reversed from those for $p < 1$. Normal, distally progressing wave solutions were found. The values of $\frac{1}{2}\lambda$ computed for $p > 1$ at various frequencies are shown in Fig. 9.

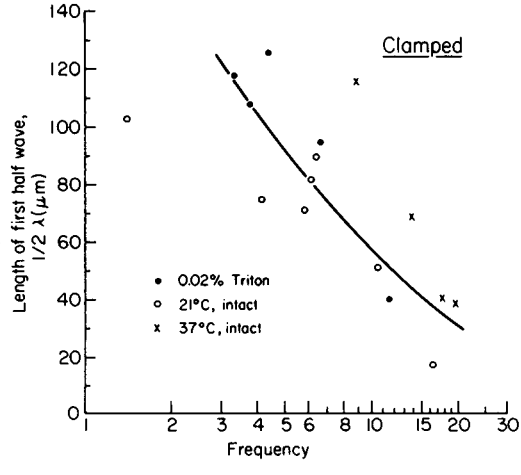

FIGURE 10 Value of $\frac{1}{2}\lambda$ of clamped bull sperm as a function of the flagellar frequency (in cycle/s). The line was drawn by eye to show the average trend of the data.

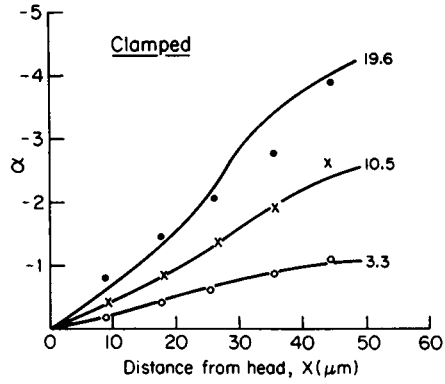

FIGURE 11 Computed $\alpha(x)$ for three clamped bull sperm at flagellar frequencies of 3.3, 10.5, and 19.6 cycle/s. •, ×, and ○ are measured points.

The measured values for $\frac{1}{2}\lambda$ for clamped bull sperm are shown in Fig. 10. The range of frequencies of approximately 2–20 cycle/s was obtained by observing sperm in various conditions (37°C, 21°C, and Triton-extracted). Fig. 10 shows that $\frac{1}{2}\lambda$ tends to be much larger at the lower frequencies. The scatter in $\frac{1}{2}\lambda$ is large and it increases towards the lower frequencies. The line drawn in Fig. 10 represents the average trend of the data. From this line, the values of p required to give the corresponding com-

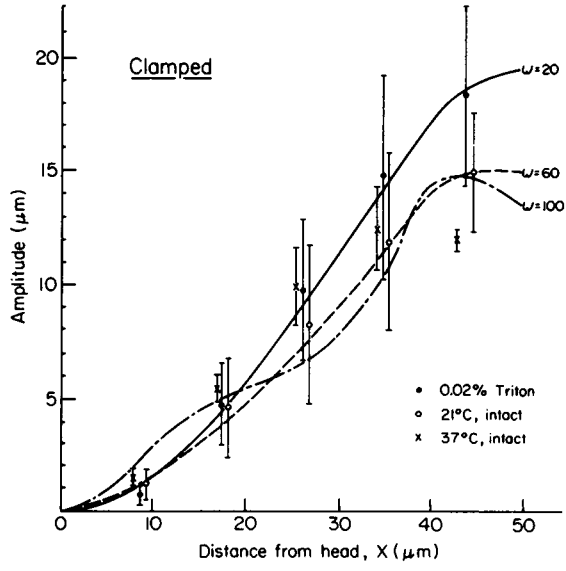

FIGURE 12 Average amplitude of the flagellar wave of clamped bull sperm in three different conditions: at 37°C, at 21°C, and Triton X-100-extracted. The vertical bars indicate standard deviations over the different sperm in each group. The lines drawn were computed for the three frequencies with the value of p indicated by the arrows in Fig. 9.

TABLE IV

STANDING MOMENT M_2, TRAVELING MOMENT M_1 AND TOTAL ACTIVE MOMENT M_{act} COMPUTED FOR CLAMPED BULL SPERM AT VARIOUS FREQUENCIES

ω	Frequency	Moments at $x = 0$		
		M_2	M_1	M_{act}
rad/s	*cycle/s*		10^{-9} *dyn cm*	
20	3.2	4.5	0.4	4.2
40	6.4	7.0	0.5	6.5
60	9.6	9.6	0.6	9.1
80	12.7	10	1.1	9.6
100	15.9	11	0.9	11
120	19.2	12	0.9	12

puted value of $\frac{1}{2}\lambda$ were derived with the aid of Fig. 9. The thus-found values of p, indicated by the arrows in Fig. 9, were all close to $p = 1.5$.

The result of the calculations as shown in Fig. 9 confirm the trend of an increasing value of $\frac{1}{2}\lambda$ with decreasing frequency, and they suggest that small variations in the magnitude of the traveling moment M_1 (as represented by p) cause the observed large scatter in $\frac{1}{2}\lambda$. The observed increase in scatter in $\frac{1}{2}\lambda$ towards smaller frequencies is also suggested by the increasing steepness of the computed curves in Fig. 9 for the lower frequencies.

The computed wave progression, expressed by the function $\alpha(x)$, is shown in Fig. 11 for three sperm at frequencies of 3.3, 10.5, and 19.6 cycle/s. The sperm were chosen to be situated close to the line drawn in Fig. 10 above. It can be seen that the computed curves for $\alpha(x)$ are very compatible with the measured points.

For live clamped bull sperm, the amplitude of the flagellar wave does not appear to vary with the frequency. Fig. 12 shows the measured amplitudes as a function of the distance from the head for the clamped sperm in the three different conditions (37°C, 21°C, Triton-extracted). The curves shown in Fig. 12 were computed for three different frequencies, chosen to represent roughly the average frequencies of the sperm in the three different groups. The appropriate value of p in each case was taken from Fig. 9, and the value of m_0 was adjusted so that the computed amplitudes agreed as well as possible to the measured ones as shown in Fig. 12. Table IV shows the value of the moments M_1, M_2, and M_{act} obtained with this procedure over the whole range of frequencies. The values for the moments shown in Table IV should be treated with caution, in view of the serious simplification of the geometry of the flagellum used in the present theory. It is probable, though, that the trend shown in Table IV of increasing moments at the higher flagellar frequencies is real.

Fig. 13 shows computed and observed wave forms of two clamped bull sperm at 6 and 20 cycle/s, respectively. Even though at the distal part of the flagella projection effects are clearly important, the general shape of the waves is reasonably well represented in the computations.

HINGED AND FREE BOUNDARY CONDITIONS With free boundary conditions

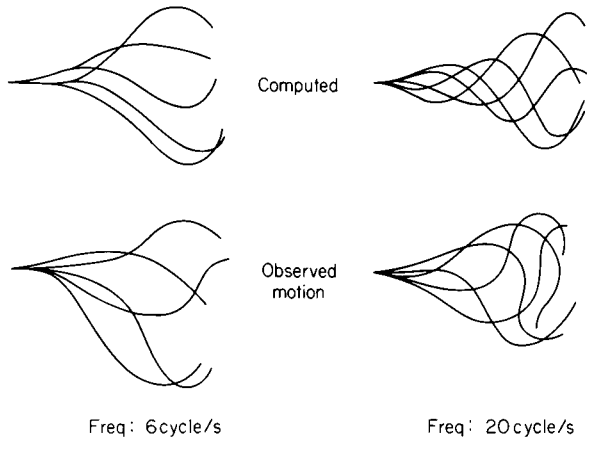

FIGURE 13 Observed and computed wave forms of clamped bull sperm with a flagellar frequency of 6 (left) and 20 cycle/s (right).

no meaningful solutions were obtained when using the values of l, δ, k, and lE defined above for bull sperm and any value of p. The proximal 10 μm of the computed solutions developed a strong curvature, leading to amplitudes >100 μm at $x = 0$, and the distal part ($10\,\mu m < x < 60\,\mu m$) showed waves of irregular amplitude and progression. This was probably due to the lack of restraints on the proximal part of the computed flagellum. In live bull sperm the extra stiffness in the midpiece ($x < 10$ μm) prevents the development of a strong curvature.

For hinged bull sperm meaningful solutions were obtained for all frequencies of the flagellar wave. Since $U(0, t) = 0$ for the hinged boundary conditions, this supports the notion that the failure to obtain solutions in the free case was due to a lack of restraints on the motion in the proximal part. It has been pointed out also (Rikmenspoel, 1966) that in flagella as stiff as those of bull sperm the influence of the restraints at the proximal junction are manifest over a large fraction of the length. In sea urchin sperm flagella, 20 times less stiff than bull sperm flagella, the influence of the boundary conditions is mainly felt in the proximal 5–10 μm of the flagella. Our present results on free bull sperm and free sea urchin sperm agree with this.

For the purpose of the present paper, the data for free and for hinged bull sperm have been compared to calculated results obtained with hinged boundary conditions. The measured values of $\frac{1}{2}\lambda$ as a function of frequency are shown in Fig. 14 for the free and hinged bull sperm. It can be seen that the two different boundary conditions have identical relations between $\frac{1}{2}\lambda$ and f. It can also be seen that the scatter in $\frac{1}{2}\lambda$ is much smaller for the free and hinged bull sperm than for the clamped ones. Fig. 15 shows the amplitude of the waves in free and hinged bull sperm as a function of the position on the flagellum. As in the case of clamped bull sperm above, no relation was found between amplitude and frequency in the waves. The data were therefore grouped in three classes, representing the sperm at 37°C and 21°C and those which were Triton-extracted. It can be seen from Fig. 14 that these groups have wave frequencies centered

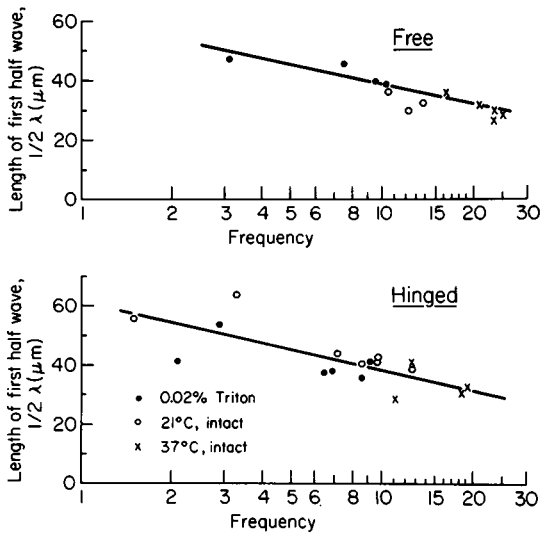

FIGURE 14 Length of first half wave ($\frac{1}{2}\lambda$) of free and hinged bull sperm as a function of the flagellar frequency (cycle/s). The lines drawn in the top and bottom graph were computed with values of p as shown in Table V.

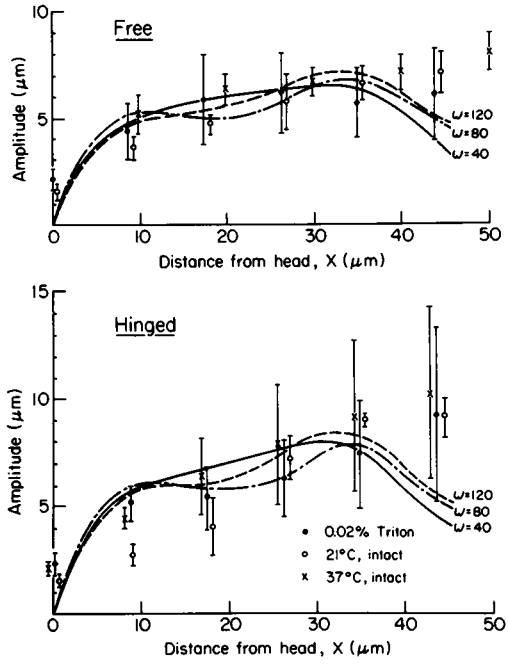

FIGURE 15 Average amplitude as a function of frequency of free and hinged bull sperm. The sperm were in three different conditions: at 37°C, at 21°C, and Triton X-100-extracted. The vertical bars represent the standard deviations within each group. The lines were computed for the three different frequencies with the value of p as shown in Table V.

TABLE V

p VALUES, STANDING MOMENT M_2, TRAVELING MOMENT M_1, AND TOTAL ACTIVE MOMENT M_{act} COMPUTED FOR HINGED BULL SPERM AT VARIOUS FREQUENCIES

ω	Frequency	p	Moments at $x = 0$		
			M_2	M_1	M_{act}
rad/s	*cycle/s*			10^{-9} *dyn cm*	
20	3.2	0.75	0.6	0.9	1.0
40	6.4	0.8	1.0	1.0	1.6
60	9.6	0.9	1.6	1.4	1.9
80	12.7	1.2	2.0	1.7	3.4
100	15.9	1.5	2.6	2.5	4.9
120	19.2	1.5	3.3	2.8	5.8

around approximately 19, 12, and 6 cycle/s, respectively. The standard deviations of the amplitude values for the three groups overlap at almost all locations on the flagellum, for the free as well as for the hinged sperm, as can be seen in Fig. 15.

Initial calculations, performed with the appropriate values for l, δ, and lE, showed that the values for $\frac{1}{2}\lambda$, computed for the hinged case, depended weakly on the value of p, as was found for free sea urchin sperm above. The computed amplitude in the distal part of the flagella increased with increasing values of p. For each frequency that value of p was found by some trial and error that gave the best shape of the variation of the amplitude with x. The value of m_0 was then adjusted such that the absolute value of the amplitude gave the best fit with the experimental points.

Table V shows the values of p for free and hinged bull sperm at various frequencies determined as described above. The lines drawn in Fig. 14, top and bottom, show the variation of $\frac{1}{2}\lambda$ with frequency, computed with p as in Table V. It can be seen that the computed curves agree well with the measured points. In Fig. 15 are shown three examples, for frequencies of 6.4 cycle/s ($\omega = 40$), 12.7 cycle/s ($\omega = 80$), and 19.1 cycle/s ($\omega = 120$), of the computed amplitude as a function of the location x on the flagellum. It can be seen in Fig. 15 that in the distal region of the flagella ($x > 40$ μm) the observed amplitudes increase. The computed values of the amplitude decrease for $x > 40$ μm, probably due to the neglected effects of the taper of the flagellum. The resistance to bending and the viscous resistance are overestimated in the computations in the distal part of the flagellum. As a result the computed amplitudes can be expected to be underestimates.

Fig. 16 shows tracings of the observed flagellar motion of two hinged sperm at 6.5 and 19 cycle/s, and of one free sperm. The flagellar profiles computed for these frequencies are also shown. Fig. 16 clearly indicates that in the proximal part (corresponding to the midpiece) the curvature of the computed shapes is much stronger than in the observed shapes. This reflects that in the computations the increased stiffness of the midpiece was not taken into account. In the distal part of the observed flagella projection effects are clearly important, and small amplitude approximation is not really valid in this region. In spite of the neglect of the variations in the structure

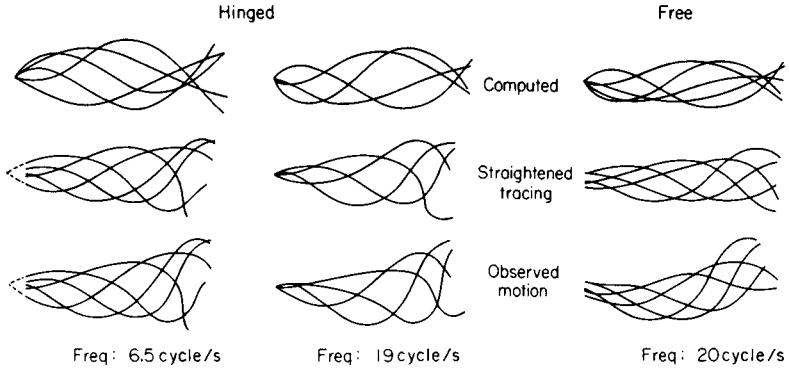

FIGURE 16 Observed and computed wave forms for two hinged bull sperm at 6.5 and 19 cycle/s and one free bull sperm at 20 cycle/s. The procedure for straightening the observed tracings is explained in the legend of Fig. 6.

along the flagellum, and of the application of small amplitude approximation, the computed wave forms are appreciably similar to the observed ones.

Table V shows the moments M_1, M_2, and M_{act}, evaluated at $x = 0$ for the computed wave forms at various frequencies. The relative magnitude of M_1 and M_2, as can be seen in Table V, remains approximately constant over the range of frequencies, even though the value of p clearly increased with frequency. It is also apparent in Table V that the total active moment M_{act} increases roughly proportionally with the frequency. Even though these moments are subject to considerable uncertainty, as in the case of clamped bull sperm above, it is probable that the trends shown in Table V are real.

Cricket Sperm

The flagellum of cricket sperm has a length of approximately 800 μm. Fig. 17 is an enlargement of a 16-mm film frame showing the proximal 280 μm of a motile cricket

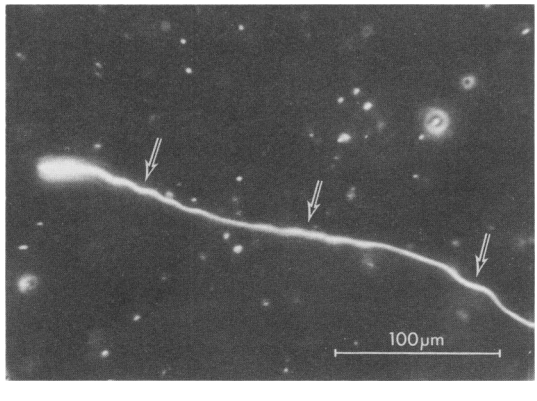

FIGURE 17 Part of a motile cricket sperm showing three sections with a different wavelength (arrows). The head of the sperm is at the left.

TABLE VI

FREQUENCY f, AMPLITUDE A, AND WAVELENGTH λ OF 12 SECTIONS ON 5 CRICKET SPERM AT NORMAL VISCOSITY

Sperm	Section	f	A	λ
		cycle/s	*μm*	*μm*
1	a	5.1	0.6	14
	b	1.4	2.5	29
2	a	12.5	0.8	7
	b	2.8	2.6	33
3	a	1.5	2.3	26.5
	b	0.6	5.3	58
4	a	2.3	2.0	28.5
	b	2.6	1.7	19
5	a	8.8	0.7	13
	b	2.8	2.6	26
	c	4.9	1.3	28
	d	9.3	1.2	10

sperm. Three different sections can be noticed on the sperm with wavelengths of 15, 20, 28 μm, respectively. Table VI shows that consistently, on a single sperm, sections with different wave parameters were observed. This shows that in these sperm the wave motion reflects the local contractile activity, and that the flagella do not move as a whole unit.

Cricket sperm were observed at a raised viscosity of 10 and 72 cP. In both these cases the same sperm showed different wave motions on different sections, as was observed at normal viscosity. Table VII shows that the average frequency, amplitude, and wavelength of the motion of cricket sperm do not vary significantly with the viscosity.

In Fig. 18 are plotted the amplitude and wavelength as a function of the frequency of the wave motion in all sections measured at the three different viscosities. Even though the spread of the data points is considerable, the amplitude and wavelength display approximately the same relation to frequency at the different viscosities. This tends to confirm that the viscous forces do not play a role in relating the wave motion to the active moment. It should be noted that this does not of course imply that the viscous forces do not play a role in the forward progression of the sperm.

TABLE VII

AVERAGE FREQUENCY $\langle f \rangle$, AVERAGE AMPLITUDE $\langle A \rangle$, AND AVERAGE WAVELENGTH $\langle \lambda \rangle$ OF CRICKET SPERM AT VARIOUS VISCOSITIES

Viscosity	No. of sperm	No. of sections	$\langle f \rangle$	$\langle A \rangle$	$\langle \lambda \rangle$
cP			*cycle/s*	*μm*	*μm*
1	5	12	4.5 ± 3.6	1.9 ± 1.3	24.2 ± 12.8
10	5	13	4.1 ± 2.3	2.9 ± 1.7	20.5 ± 9.6
72	4	9	6.0 ± 3.2	2.4 ± 1.1	17.4 ± 7.4

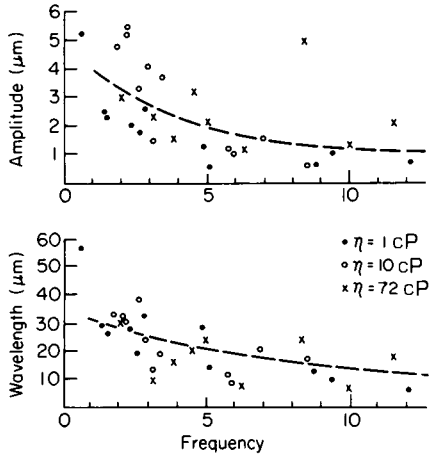

FIGURE 18 Amplitude (top) and wavelength (bottom) as a function of frequency (in cycles per second) of various sections on cricket sperm. The data were taken at three different viscosities of 1 cP (•), 10 cP (○), and 72 cP (X). The lines were drawn by eye through the points.

The above observations indicate that the long insect sperm represent indeed the case of a contractile mechanism in which the standing active moment is negligibly small. The simplified equation of motion (Eq. 27) should be adequate to describe the flagellar motility of these sperm.

DISCUSSION

The theory developed in this paper was most successful in the case of the invertebrate sperm. For these sperm an almost quantitative description of the wave forms at different frequencies and at raised viscosity was obtained. It should be kept in mind that the two basic approximations made in the theory, a cylindrical flagellum and the use of small amplitude approximation, are valid for the invertebrate sperm.

For bull sperm the computed wave shapes showed a curvature near the head-midpiece junction much larger than the observed one (Fig. 16 above). This clearly indicates that the increased stiffness caused by the midpiece structure (and neglected in the approximation of the flagellum as a cylinder with a uniform stiffness) restrains the motion near the proximal junction. A refinement of the theory, which takes into account the extra stiffness of the midpiece, and also the influence of the taper of the flagellum on the elastic bending resistance and the viscous resistance in the distal part of the flagellum, can easily be made. It would be interesting to find whether this refinement would lead to a better shape of the computed wave forms, and to meaningful wave forms in the free case. The purposes of the present paper have been, however, to investigate how much could be accomplished by a theory without any refinements or modeling.

The question can obviously be asked whether the theory developed in this paper is applicable to cellular flagella. It should be noted that the separation of variables, ap-

parent in the expression for the active moment of Eq. 7, is only possible when the flagellar wave can be expressed in one single frequency, as in Eq. 4. If the transversal motion of the flagellum is not sinusoidal in time the expression for $U(x,t)$ shows a multiple frequency spectrum:

$$U(x,t) = \sum_m \sum_n A_{nm} e^{i(\omega_m t + \alpha_n x)}.$$

The development of the theory as outlined in this paper is then no longer possible.

It would appear that for cellular flagella that show a single frequency in their transversal motion, such as *Crithidia* (Holwill, 1965), the theory should be applicable. For flagella such as those of *Euglena* or *Chlamydomonas* which show a transversal motion not sinusoidal in time, the mechanisms discussed in this paper should not be valid.

Cellular flagella can be considered to be clamped in the cell body. The finding (see Fig. 9) that it is possible to change with clamped boundary conditions the direction of the flagellar wave by a change in the ratio of the standing to the traveling moment suggests an interesting mechanism for the reversal of flagellar waves in organisms such as *Crithidia*.

In sea urchin sperm flagella it has been shown that a sliding filament mechanism, in which cross-bridges between the tubulin fibers are formed by the dynein molecules, produces the active contractile forces. It has been discussed previously (Rikmenspoel, 1971; Rikmenspoel and Rudd, 1973) that a sliding filament mechanism can be coordinated in a simple way to produce active moments of the correct form required for the sperm flagellar motion, as given in Eqs. 12 and 23 above. For bull spermatozoa the force-producing mechanism has not yet been clearly identified. The presence of the dynein-tubulin system in bull sperm flagella makes it probable that at least a part of the active contractile moment is produced by it. The outer coarse fibers in bull sperm flagella have been assumed to be force-producing by some investigators (Fawcett and Phillips, 1970; Rikmenspoel, 1971; Nelson, 1962). Others have proposed that these coarse fibers have only an elastic function (Phillips, 1972; Lindemann and Gibbons, 1973). It appears that a clearer biological identification of the contractile mechanism in bull sperm flagella should be awaited before speculations as to its coordinating mechanism could be profitable.

The experimental results obtained on cricket sperm appear to confirm that these long insect sperm represent the case of a vanishingly small standing moment discussed in the Theory section above. For these sperm the active moment consists probably only of the traveling moment M_1, given in Eq. 8. For a section on an insect sperm showing a wave with amplitude A and wave number α it is thus appropriate to write:

$$M_{act} = M_1 = A\alpha^2 e^{i(\omega t + \alpha x)}[IE + ik\omega/\alpha^4]. \quad (28)$$

The long insect sperm have the axoneme surrounded by nine auxiliary fibers (Kaye, 1964; Warner, 1970), analogous to those in the bull sperm flagellum. The auxiliary fibers in the insect sperm are somewhat thinner than those in bull sperm, however.

The stiffness of sperm flagella has been found to correlate with the thickness of the auxiliary fibers (Phillips, 1972). The value of the stiffness IE for the long insect flagella is thus intermediate between that of an axoneme (10^{-13} dyn cm^2) and that of a bull sperm flagellum (1.8×10^{-12} dyn cm^2). For the long insect sperm, $IE = 3\text{–}10 \times 10^{-13}$ dyn cm^2 can be taken as an approximate value.

For insect sperm typical values for the drag coefficient $k \approx 2 \times 10^{-2}$ dyn cm^{-2} s, the wave number $\alpha = 2\pi/\lambda = 3 \times 10^3$ cm^{-1}, and $\omega = 2\pi f = 3 \times 10^1$ s^{-1} can be adopted with Table VII above. This leads to a value of $k\omega/\alpha^4 \approx 8 \times 10^{-15}$ dyn cm^2 for the insect sperm, approximately two orders of magnitude smaller than the value of IE derived above. In Eq. 28 the second term in the square brackets can therefore be neglected compared to the first one for the insect sperm under consideration, and we can write $M_1 = A\alpha^2 IE \exp i(\omega t + \alpha x)$.

Since from Eq. 4 in the Theory section $IE\,\partial^2 U/\partial x^2 = -A\alpha^2 IE \exp i(\omega t + \alpha x)$, we find $IE(\partial^2 U/\partial x^2) + M_1 = 0$, identical to Eq. 27 in the Theory section. The drag coefficient k, no longer occurs for the long insect sperm in the expression for M_1, however. This indicates that mechanochemical feedback from the external fluid onto the contractile system in the flagella of these sperm should be essentially absent. The oscillatory system represented by the oscillating contractile mechanism in the long insect sperm can therefore probably be considered as a purely chemical oscillator (Chance et al., 1973). The observation that the frequency of the flagellar motion in these sperm does not vary over a wide range of external viscosities (1–70 cP), as shown in Table VII, tends to confirm this.

The typical value of $\alpha = 3 \times 10^3$ cm^{-1} for the cricket sperm leads to $1/\alpha^2 \approx 10^{-7}$ cm^2. With a flagellar length $l = 800\ \mu\text{m} = 8 \times 10^{-2}$ cm, a typical value for l/α is thus 2.7×10^{-5} cm^2. Since $(l - x)/\alpha$ in Eq. 25 has the same magnitude as l/α, we find that in Eq. 25 the magnitude of the second term within the square brackets is more than two orders smaller than that of the first one. The second term can therefore be neglected compared to the first one, and Eq. 25 reduces to:

$$M_2 = -k\omega A\, e^{i(\omega t + \alpha l)}\, \frac{(l - x)}{\alpha}. \tag{29}$$

Analogously, the expression for the viscous moment M_{visc} in Eq. 26 becomes in the present case:

$$M_{visc} = -k\omega A\, e^{i(\omega t + \alpha l)}\, \frac{(l - x)}{\alpha}. \tag{30}$$

The equation of motion 1 can be written as, with $M_{act} = M_1 + M_2$,

$$M_{el} + M_1 + M_2 = M_{visc} \tag{31}$$

Since from Eqs. 29 and 30, $M_2 = M_{visc}$, and with $M_{el} = IE\,\partial^2 U/\partial x^2$, the equation of motion 31 becomes in the present case $IE(\partial^2 U/\partial x^2) + M_1 = 0$: again Eq. 27.

In the above derivation of Eq. 27 only the condition $1/\alpha \ll l$ has in fact been used.

The elimination of M_{visc} has occurred because M_{visc} cancels against M_2. The validity of Eq. 27 thus does not depend on a complete absence of standing moment in the flagella.

Since Eq. 27 does not contain a term representing the standing moment, the presence of a small amount of standing moment will not manifest itself in the motion of a flagellum for which the equation is valid. The motion parameters of the flagellum then cannot be used to determine the amount of standing moment present in the flagellum.

It is to be expected that the theoretical treatment given in this paper loses validity when the standing moment produced in a long insect flagellum is comparable to or exceeds the magnitude of the right-hand side of Eq. 29. For the cricket sperm, typical values were $k = 2 \times 10^{-2}$ dyn cm^{-2} s, $\omega = 30$ s^{-1}, $A = 4 \times 10^{-4}$ cm, $l = 8 \times 10^{-2}$ cm, and $\alpha = 3 \times 10^{3}$ cm^{-1}. The value of the maximum amount of standing moment that could be present in a cricket sperm without violating the validity of Eq. 27 would thus be $k\omega Al/\alpha$, or approximately 6×10^{-9} dyn cm. A comparison with the magnitudes of the standing moments found in sea urchin and bull sperm (Tables II, III, and V) shows that the upper limit for the standing moment allowed in the long insect sperm is not critically low. Since the observations indicate that Eq. 27 is very well obeyed by the cricket sperm, the standing moment present in these sperm is probably at least one order of magnitude smaller than the upper limit derived above.

According to Eq. 27, the traveling active moments in the long insect sperm flagella are directly displayed in the flagellar wave motion. Detailed descriptions of the motion in various experimental conditions could yield probably the most direct information on the kinetics of the contractile processes in these sperm. Such descriptions have apparently not been published in the literature.

One of the main results of the theory in this paper has been that without a standing moment involving the whole flagellum as a unit, no wave solutions with a wavelength comparable to the flagellar length are possible. This leads to the distinction between the class of sperm that display approximately one full wave in the flagellum (invertebrates, mammalian), and the class with many small waves (insect). To my knowledge no cases have been described that could be regarded as intermediates, displaying for example three to four waves on the flagellum. The lack of these intermediate forms can be taken as supporting the basis of the present theory.

My thanks are due to Dr. Angelo Skalafuris, who first pointed out the method for solving the equation of motion employed in this paper. The many helpful discussions with Dr. Charles Lindemann and Dr. Kathleen Nichols are gladly acknowledged. Mrs. Sandra Orris, Mrs. Alice Jacket, and Miss Elizabeth Naismith are thanked for assistance with the experimental work and the running of the computer programs.

This investigation was supported in part by the National Institute of Child Health and Human Development through grants HD-8752 and HD-6445.

Received for publication 26 September 1977 and in revised form 19 March 1978.

APPENDIX

The transformation $X = x/l$ results in a dimensionless running coordinate with a range $0 \leq X \leq 1$, and in dimensionless wave numbers $\kappa_n = \alpha_n l$. The length of the flagellum becomes the

dimensionless number 1. After the transformation the expression for the standing moment M_2 given in Eq. 9 of the text becomes:

$$M_2 = - e^{i\omega t} \sum_n k\omega A_n \frac{e^{i\kappa_n}}{\kappa_n} l^2 \left[(1 - X) + \frac{i}{\kappa_n}\right]. \quad \text{(A1)}$$

For a particular wave solution with a (finite) A and a wave number κ, Eq. A1 can be rewritten as:

$$M_2 = - k\omega A l^2 e^{i(\omega t + \kappa)} \left[\frac{1 - X}{\kappa} + \frac{i}{\kappa^2}\right] \quad \text{(A2)}$$

For M_2 to vanish, both terms within the square brackets in Eq. A2 must vanish, and therefore $1/\kappa$ must be $\ll 1$. A *necessary* condition for the vanishing of M_2 is thus, with $1/\alpha = l/\kappa$,

$$1/\alpha \ll l \quad \text{(A3)}$$

It should be noted that Eq. A3 is not a sufficient condition. A sufficient condition requires the specification of a (small) number ϵ, and the condition $1/\kappa < \epsilon$ (which then also fulfills $1/\kappa^2 < \epsilon$).

The cricket sperm treated in this paper had a length $l \approx 800\ \mu$m. The typical wavelength λ in these sperm is $\approx 20\ \mu$m, leading to $\alpha = 2\pi/\lambda = 0.3\ \mu\text{m}^{-1}$. The value of $\kappa = \alpha l$ for cricket sperm is thus ≈ 240 and $1/\kappa \approx 0.4 \times 10^{-2}$. Assuming that these cricket sperm do indeed represent a case in which the standing moment M_2 has become negligible, an appropriate value for ϵ then would probably be $\epsilon = 10^{-2}$.

Since $(l - x)/\alpha < l/\alpha = l^2/\kappa$, and with $1/\alpha^2 = l^2/\kappa^2$, the sufficient condition $1/\kappa < \epsilon$ (and therefore $1/\kappa^2 < \epsilon$) is equivalent to the condition $(l - x)/\alpha < \epsilon l^2$ and $1/\alpha^2 < \epsilon l^2$. In the text, under The Traveling Moment, the expression "sufficiently small" is used instead of "$< \epsilon l^2$" as defined above.

REFERENCES

AFZELIUS, B. A., editor. 1974. The functional anatomy of the spermatozoon. Pergamon Press, Inc., Elmsford, N.Y. 393 pp.

BROKAW, C. J. 1966. Effects of increased viscosity on the movements of some invertebrate spermatozoa. *J. Exp. Biol.* **45**:113–139.

BROKAW, C. J. 1972*a*. Computer simulation of flagellar movement. I. Demonstration of stable bend propagation and bend initiation by the sliding filament model. *Biophys. J.* **12**:564–586.

BROKAW, C. J. 1972*b*. Computer simulation of flagellar movement. II. Influence of external viscosity on movement of the sliding filament model. *J. Mechanochem. Cell Motility.* **1**:203–212.

BROKAW, C. J. 1974. Movement of the flagellum of some marine invertebrate spermatozoa. *In* Cilia and Flagella. M. A. Sleigh, editor. Academic Press, Inc., New York. 93–110.

BROKAW, C. J. 1975. Spermatozoan motility: a biophysical survey. *Biol. J. Linn. Soc.* **7**:423–439.

BROKAW, C. J., and D. R. RINTALA. 1974. Computer simulation of flagellar movement. III. Models incorporating crossbridge kinetics. *J. Mechanochem. Cell Motility.* **3**:77–86.

CHANCE, B., E. K. PYE, A. K. GHOSH, and B. HESS, editors. 1973. Biological and Biochemical Oscillators. Academic Press, Inc., London and New York. 534 pp.

CHAPMAN, R. F. 1969. The Insects: Structure and Function. English Universities Press Ltd., London.

FAWCETT, D. W. 1961. Cilia and flagella. *In* The Cell. J. Brachet and A. E. Mirsky, editors. Academic Press, Inc., New York and London. Vol. II, 217–298.

FAWCETT, D. W. 1966. The Cell: Its organelles and Inclusions. W. B. Saunders Company, Philadelphia. 448.

FAWCETT, D. W. and D. M. PHILLIPS. 1970. Recent observations on the ultrastructure and development of the mammalian spermatozoon. *In* Comparative Spermatology. B. Baccetti, editor. Academic Press, Inc., New York and London. 13–28.

FIELDEN, A. 1960. Transmission through the last abdominal ganglion of the dragonfly nymph Anax imperator. *J. Exp. Biol.* **37**:832–846.

GIBBONS, I. R. 1974. Mechanisms of flagellar motility. *In* The Functional Anatomy of the Spermatozoon, B. A. Afzelius, editor. Pergamon Press, Inc., Elmsford, N.Y. 127–140.

GRAY, J. 1955. The movement of sea urchin spermatozoa. *J. Exp. Biol.* **32**:775–801.

GRAY, J., and G. J. HANCOCK. 1955. The propulsion of sea urchin spermatozoa. *J. Exp. Biol.* **32**:802–814.

HOLWILL, M. E. J. 1965. The motion of *Strigomonas oconpelti*. *J. Exp. Biol.* **42**:125–137.

KAYE, J. S. 1964. The fine structure of flagella in spermatids of the house cricket. *J. Cell Biol.* **22**:710–714.

LINDEMANN, C. B. 1975. An analytical measurement of the stiffness of intact and demembranated sea urchin sperm during motility. *Biophys. J.* **15**:160*a*. (Abstr.).

LINDEMANN, C. B., and I. R. GIBBONS. 1975. Adenosine triphosphate induced motility and sliding filaments in mammalian sperm extracted with Triton X-100. *J. Cell Biol.* **65**:147–162.

LINDEMANN, C. B., and R. RIKMENSPOEL. 1971. Intracellular potentials in bull spermatozoa. *J. Physiol. (Lond.).* **219**:127–138.

LINDEMANN, C. B., and R. RIKMENSPOEL. 1972. Simple viscometer for samples less than 1 ml. *J. Sci. Instrum.* **5**:178–180.

LINDEMANN, C. B., W. G. RUDD, and R. RIKMENSPOEL. 1973. The stiffness of the flagella of impaled bull sperm. *Biophys. J.* **13**:437–448.

LUBLINER, J., and J. J. BLUM. 1971. Model for bend propagation in flagella. *J. Theor. Biol.* **31**:1–24.

LUBLINER, J., and J. J. BLUM. 1972. Analysis of form and speed of flagellar waves according to a sliding filament model. *J. Mechanochem. Cell. Motility.* **1**:157–167.

MACHIN, K. E. 1958. Wave propagation along flagella. *J. Exp. Biol.* **35**:796–804.

NELSON, L. 1962. Cytochemical aspects of spermatozoan motility. *In* Spermatozoan Motility, D. W. Bishop, editor. American Association for the Advancement of Science, Washington, D.C. 171–187.

PHILLIPS, D. M. 1970. Insect sperm: their structure and morphogenesis. *J. Cell Biol.* **44**:243–277.

PHILLIPS, D. M. 1972. Comparative analysis of mammalian sperm motility. *J. Cell Biol.* **53**:561–573.

PHILLIPS, D. M. 1974. Structural variants in invertebrate sperm flagella and their relationship to motility. *In* Cilia and Flagella, M. A. Sleigh, editor. Academic Press, Inc., New York and London. 379–402.

RIKMENSPOEL, R. 1965. The tail movement of bull spermatozoa. Observations and model calculations. *Biophys. J.* **5**:365–392.

RIKMENSPOEL, R. 1966. Elastic properties of the sea urchin sperm flagellum. *Biophys. J.* **6**:471–479.

RIKMENSPOEL, R. 1971. Contractile mechanisms in flagella. *Biophys. J.* **11**:446–463.

RIKMENSPOEL, R. 1976. Contractile events in the cilia of *Paramecium, Opalina, Mytelus,* and *Phragmatopoma. Biophys. J.* **16**:445–470.

RIKMENSPOEL, R. 1978. The movement of sea urchin sperm. *J. Cell Biol.* **76**:310–322.

RIKMENSPOEL, R., and W. G. RUDD. 1973. The contractile mechanism in cilia. *Biophys. J.* **13**:955–993.

RIKMENSPOEL, R., A. C. JACKLET, S. E. ORRIS, and C. B. Lindemann. 1973. Control of bull sperm motility. Effects of viscosity, KCN and thiourea. *J. Mechanochem. Cell Motility.* **2**:7–24.

SATIR, P. 1968. Studies on cilia. III. Further studies of the cilium tip and a "sliding filament" model of ciliary motility. *J. Cell Biol.* **39**:77–94.

SKALAFURIS, A. J., and R. RIKMENSPOEL. 1973. Flagellar wave motion driven by a linear simultaneous active moment. *Biophysical Society Abstracts.* **13**:212*a*. (Abstr.).

SUMMERS, K. E., and I. R. GIBBONS. 1971. Adenosine triphosphate induced sliding of tubules in trypsin-treated flagella of sea urchin sperm. *Proc. Natl. Acad. Sci. U.S.A.* **68**:3092–3096.

WARNER, F. 1970. New observations on flagellar fine structure. *J. Cell Biol.* **47**:159–182.

WU, T. Y. T., C. J. BROKAW, and C. BRENNEN, editors. 1975. Swimming and Flying in Nature. Vol. 1. Plenum Publishing Corporation, New York and London. 421 pp.